A computer program for interconversion between creep compliance and stress relaxation

Sachin Shanbhag*

Department of Scientific Computing, Florida State University, Tallahassee, FL 32306. USA

(Dated: June 28, 2023)

Abstract

Numerical interconversion of linear viscoelastic functions is an important problem in rheology. This work focuses on interconversion between creep compliance (J) and relaxation modulus (G) via the convolution relation. A discrete spectrum or Prony series is used to describe both the source (G or J) and the target (J or G) of the interconversion. A previously developed numerical template [Loy et al., *J. Rheol.*, **59**(5):1261, (2015)] is modified to bypass singularities. It is released as an open-source computer program called PSI (Prony series interconversion). PSI is tested on a variety of materials including viscoelastic solids and liquids, and used for both $G \to J$ and $J \to G$ interconversions. It is fast and numerically stable for input data that span over twenty decades in time. It fills a gap in the existing software landscape for conversion of linear viscoelastic functions.

I. INTRODUCTION

Different linear viscoelastic (LVE) functions spotlight different aspects of material structure and dynamics. For example, among time (t) dependent LVE functions, it is well-known that the relaxation modulus $G(t)$ emphasizes short time relaxation processes, while creep compliance $J(t)$ is more sensitive to long-time relaxation behavior [1–3]. With perfect and complete information, all LVE functions are mathematically equivalent; the choice of which function to use is a question of preference or ease of measurement. For example, $G(t)$ is the natural output of many theories and simulations of polymer melts [4–8]. On the other hand, measuring $G(t)$ of asphalt mixtures is challenging, while $J(t)$ can be determined with more ease and accuracy [9, 10].

There is often a practical need to convert computational or experimental LVE observations, which are typically noisy and limited to a finite time or frequency window, to other LVE functions. For instance, in order to compare theories of polymer melts with experimental data, $G(t)$ computed from simulations has to be converted to the dynamic modulus $G^*(\omega)$, which is usually the object of experimental investigations. Similarly, to predict thermal stresses in asphalt pavements using finite element modeling software, the observed $J(t)$ has to be converted to $G(t)$ [9, 11]. Unsurprisingly, analytical and numerical methods for interconversion between different LVE functions is a classic problem in rheology with a long and rich tradition [1, 2, 12].

In this work, we focus on one of these problems, viz. the interconversion between $G(t)$ and

* sshanbhag@fsu.edu

$J(t)$. These functions are mathematically related via a convolution relation which takes the form of a Volterra equation of the first kind [1, 2, 13],

$$t = \int_0^t J(t')\,G(t-t')\,dt' = \int_0^t G(t')\,J(t-t')\,dt', \quad t \geq 0. \tag{1}$$

Numerical integration of this equation requires special care, and many standard quadrature methods do not work well [2, 14–17]. Sorvari and Malinen [18] argued that the best numerical scheme might be the midpoint method, which is second-order accurate. In numerical integration, the domain of integration is divided into subintervals over which the target function (say J) is assumed to be constant or linear, and integration over the source function (say G) is performed numerically or analytically. It leads to a triangular system of linear equations, which, in principle can be solved efficiently [19]. Unfortunately, the resulting system is ill-conditioned and highly susceptible to perturbations. Stabilization using a technique like Tikhonov regularization is necessary to produce meaningful results [18, 20].

An alternative approach that avoids numerical integration considers the Laplace transform of equation 1 to obtain a simpler form of the convolution relation,

$$\tilde{J}(s)\,\tilde{G}(s) = 1/s^2, \tag{2}$$

where the Laplace transform of a function $f(t)$ is defined as $\tilde{f}(s) = \int_0^\infty f(t)e^{-st}dt$. The primary obstacle with this formulation is that numerically inverting Laplace transforms is a difficult problem [20–22]. Nevertheless, we can represent $J(t)$ and $G(t)$ using a Prony series – a weighted sum of decaying exponentials [23]. Since the Laplace transform of $e^{-\alpha t}$ with real $\alpha \geq 0$ is $(s+\alpha)^{-1}$, this representation recasts the interconversion problem into a set of algebraic equations. Several methods have been proposed to extract the parameters of the target Prony series [2, 20, 24–31].

A. Prony Series Representation

The most general form of the Prony series for $J(t)$ that includes both viscoelastic solids and liquids is,

$$J(t) = J_e + \eta_0^{-1}t - \sum_{k=1}^{n} j_k e^{-t/\lambda_k}, \tag{3}$$

where the inverse viscosity (or fluidity) η_0^{-1} is zero for solids, and nonzero for liquids. J_e is the common symbol used to denote the equilibrium compliance $J(t\to\infty)$ for solids, and the steady-state compliance, $\lim_{t\to\infty} J(t) - \eta_0^{-1}t$ for liquids. The set of modes $\{j_k, \lambda_k\}_{k=1}^n$ constitute the *discrete*

retardation spectrum, where the coefficients j_k indicate the strength of the kth mode characterized by the retardation timescale λ_k. All these parameters $\{j_k, \lambda_k\}_{k=1}^{n}$, J_e, and η_0^{-1} are non-negative. Since, $J(t=0) = J_e - \sum_k j_k \geq 0$, we additionally require $J_e \geq \sum_k j_k$.

In like manner, the most general form of the Prony series for $G(t)$ can be written as,

$$G(t) = G_e + \sum_{k=1}^{n} g_k e^{-t/\tau_k} \tag{4}$$

where G_e is the equilibrium modulus. The set of modes $\{g_k, \tau_k\}_{k=1}^{n}$ constitute the discrete relaxation spectrum, where g_k indicates the strength of the kth mode characterized by the relaxation timescale τ_k. $G_e > 0$ for solids, and $G_e = 0$ for liquids. From the convolution relation it follows that,

$$G(0)J(0) = G(\infty)J(\infty) = 1. \tag{5}$$

When we take the Laplace transforms of the Prony series representations (equations 3 and 4), and substitute them into the convolution relation (equation 2), the target LVE function ($\tilde{J}(s)$ or $\tilde{G}(s)$) is obtained as a rational function. Building on prior work [20, 24, 25, 32], Loy et al. [31] developed an elegant two-stage numerical method to obtain the target Prony series using this formulation for both viscoelastic solids and liquids. First, the time constants of the target LVE function (τ_k or λ_k) are resolved by exploiting an interlacing property. The coefficients (g_k or j_k) are subsequently determined using explicit algebraic relations. This method can be used to convert $G(t)$ to $J(t)$, or vice versa, although it is understood that the conversion $J \to G$ is computationally more challenging than $G \to J$ [15, 17, 33–35]. In this work, the notation $J \to G$ denotes interconversion of the source LVE function $J(t)$ to the target LVE function $G(t)$. Similarly, $G \to J$ denotes interconversion of $G(t)$ to infer $J(t)$.

Fortunately, if the discrete spectrum characterizing the source LVE function is parsimonious, and the time constants are well-separated, then empirically we find that the interconversion relations do not result in a severely ill-conditioned problem [17, 20, 27, 33–35]. A judiciously chosen Prony series has a regularizing effect, suppresses numerical instability [17], and makes it possible to perform interconversion.

B. Motivation and Scope

While several dozen papers have been published on numerical algorithms for interconversion between $G(t)$ and $J(t)$ over the years, it has not resulted in corresponding computer software that

is widely available or used. Given the pervasive nature of this problem, the primary goal of this work is to fill that gap. We present a free and open-source python program PSI which stands for Prony Series Interconversion.

PSI is primarily based on the method presented in Loy et al. [31], and can be used to convert $G(t)$ to $J(t)$, and vice versa. For brevity, we refer to their work as LdHA through the rest of this work, after the initials of the authors. We modify the method proposed by LdHA by introducing a small mathematical trick to avoid singularities, that turns out to be computationally convenient. This difference between PSI and LdHA is discussed in section II. As a starting point, we assume that a parsimonious spectrum corresponding to the source function or data is available. If not, a free and open-source computer program like pyReSpect, previously developed in our group, may be used [36–38]. Alternative software to extract parsimonious discrete spectra include programs like IRIS (Interactive Rheology Information System) [25], or DISCRETE [39]. Links to all the software programs mentioned above are provided in the supplementary material (see "Links to Software" section).

In section II, we summarize the LdHA method, and reproduce relevant equations using more standard rheological notation. We validate the computer program PSI using five different test problems. We find that PSI is computationally fast, and works well on a wide range of materials and problems. We look for the onset of numerical instability, and find that PSI is stable for input data that span over twenty decades in time. This range covers most experimental or simulation data reported in the literature.

II. METHODS

We begin by reviewing mathematical properties that are important for Prony series interconversion [31, 32].

1. **Prony Series Parameters**: The number of discrete modes or summands in the source function automatically determines the number of summands in the target function [31, 32]. Relationships for both viscoelastic solids and liquids are summarized in Table I.

   For solids, the number of parameters characterizing the Prony series is $2N+1$ for both $G(t)$ and $J(t)$. This includes $2N$ parameters corresponding to the coefficients (g_k or j_k) and time constants (τ_k or λ_k) of the discrete spectrum, and additionally G_e or J_e. Recall that

property	solid	liquid
$G(t)$	$G_e + \sum_{k=1}^{N} g_k e^{-t/\tau_k}$	$\sum_{k=1}^{N} g_k e^{-t/\tau_k}$
$J(t)$	$J_e - \sum_{k=1}^{N} j_k e^{-t/\lambda_k}$	$J_e + \eta_0^{-1} t - \sum_{k=1}^{N-1} j_k e^{-t/\lambda_k}$
# parameters	$2N+1$	$2N$
$\tilde{G}(s)$	$\frac{G_e}{s} + \sum_{k=1}^{N} \frac{g_k}{s+\alpha_k}$	$\sum_{k=1}^{N} \frac{g_k}{s+\alpha_k}$
$\tilde{J}(s)$	$\frac{J_e}{s} - \sum_{k=1}^{N} \frac{j_k}{s+\beta_k}$	$\frac{J_e}{s} + \frac{\eta_0^{-1}}{s^2} - \sum_{k=1}^{N-1} \frac{j_k}{s+\beta_k}$

TABLE I. Prony series representations for $G(t)$ and $J(t)$, and their Laplace transforms have the same total number of parameters. Reciprocal relaxation and retardation times are denoted by $\alpha_k = 1/\tau_k$ and $\beta_k = 1/\lambda_k$, respectively.

$\eta_0^{-1} = 0$ for solids. For liquids, the corresponding number of parameters is $2N$. For $G(t)$ this corresponds to $\{g_k, \tau_k\}_{k=1}^{N}$. Interestingly, the corresponding discrete spectrum for $J(t)$ only has $N-1$ modes, viz. $\{j_k, \lambda_k\}_{k=1}^{N-1}$ for a total of $2N-2$ parameters. The remaining two parameters are J_e and η_0^{-1}.

2. Roots and Poles of Laplace Transforms

Table I also shows the corresponding Laplace transforms, which retain the same set of Prony series parameters. It is convenient to introduce the reciprocal relaxation and retardation times as $\alpha_k = 1/\tau_k$ and $\beta_k = 1/\lambda_k$, respectively. From the Laplace transforms in Table I, we find that the negative reciprocal times $\{-\alpha_k\}$ and $\{-\beta_k\}$ constitute the nonzero poles of $\tilde{G}(s)$ and $\tilde{J}(s)$, respectively.

An important property of the Prony series representation is that the roots of $\tilde{G}(s)$ occur at the nonzero poles of $\tilde{J}(s)$ [20, 25, 31, 32]. Thus,

$$\tilde{G}(-\beta_k) = 0, \qquad 1 \le k \le n. \tag{6}$$

where $n = N-1$ for liquids, and $n = N$ for solids. Similarly, the roots of $\tilde{J}(s)$ occur at the nonzero poles of $\tilde{G}(s)$,

$$\tilde{J}(-\alpha_k) = 0, \qquad 1 \le k \le N. \tag{7}$$

3. **Interlacing Property**: If relaxation and retardation times are sorted in ascending order, the interlacing property states that the relaxation and retardation times interleave, i.e.,

$$\begin{aligned} \text{solids: } & 0 < \tau_1 < \lambda_1 < \tau_2 < \cdots < \lambda_{N-1} < \tau_N < \lambda_N < \infty \\ \text{liquids: } & 0 < \tau_1 < \lambda_1 < \tau_2 < \cdots < \lambda_{N-1} < \tau_N < \infty. \end{aligned} \tag{8}$$

In terms of reciprocal relaxation or retardation times, this translates to,

$$\begin{aligned} \text{solids: } & \infty > \alpha_1 > \beta_1 > \alpha_2 > \cdots > \beta_{N-1} > \alpha_N > \beta_N > 0 \\ \text{liquids: } & \infty > \alpha_1 > \beta_1 > \alpha_2 > \cdots > \beta_{N-1} > \alpha_N > 0. \end{aligned} \tag{9}$$

This property is practically useful as it brackets unknown time constants of the target function between the known time constants of the source function, allowing us to use a method like bisection for root finding [19].

Equipped with these mathematical properties, LdHA proposed an elegant two-step algorithm. In the first step, the reciprocal relaxation or retardation times are determined. For concreteness, consider the $G \to J$ conversion. In this case, the parameters $\{g_k, \tau_k, G_e\}$ are known, and we can form the rational function corresponding to the Laplace transform $\tilde{G}(s)$ using the appropriate relation from Table I. From equation 6, the roots of $\tilde{G}(s)$ yield $\{-\beta_k\}$ from which the retardation time constants λ_k can be obtained. The search for the roots is facilitated by the interlacing property (equation 8). In the second step, all other parameters and coefficients of the target function are determined using explicit relations summarized in Table II [31].

A. Algorithmic Differences in PSI

Table II is analogous to a similar table in LdHA; however, it explicitly identifies what is known and what is unknown for different materials (solids or liquids), and uses more traditional rheological nomenclature for Prony series parameters. For example, the symbol j_0 in LdHA refers to J_e for solids and η_0^{-1} for liquids. By being more verbose, the presentation in Table II avoids potential confusion.

We caution against an instructive corner case encountered when $J(0) = 0$. This may occur for power-law materials like critical gels where $J(t) \propto t^m$ [40]. In such cases, $J_e = \sum_k j_k$, and a potential problem arises in going from $J \to G$ as one of the roots disappears. Alternatively, this

G → J		
	solids	*liquids*
input	$G_e, \{g_k, \alpha_k\}_{k=1}^N$	$\{g_k, \alpha_k\}_{k=1}^N$
solve $\tilde{G}(s) = 0$	$\{\beta_k\}_{k=1}^N$	$\{\beta_k\}_{k=1}^{N-1}$
unknowns left	$J_e, \{j_k\}_{k=1}^N$	$J_e, \eta_0^{-1}, \{j_k\}_{k=1}^{N-1}$
J_e	$1/G_e$	$\left(\sum_{k=1}^N \frac{g_k}{\alpha_k}\right)^{-2}\left(\sum_{k=1}^N \frac{g_k}{\alpha_k^2}\right)$
η_0^{-1}		$\left(\sum_{k=1}^N \frac{g_k}{\alpha_k}\right)^{-1}$
j_k	$\left(G_e + \sum_{i=1}^N \frac{g_i\beta_k^2}{(\alpha_i-\beta_k)^2}\right)^{-1}$	$\left(\sum_{i=1}^N \frac{g_i\beta_k^2}{(\alpha_i-\beta_k)^2}\right)^{-1}$
J → G		
input	$J_e, \{j_k, \lambda_k\}_{k=1}^N$	$J_e, \eta_0^{-1}, \{j_k, \lambda_k\}_{k=1}^{N-1}$
solve $\tilde{J}(s) = 0$	$\{\alpha_k\}_{k=1}^N$	$\{\alpha_k\}_{k=1}^N$
unknowns left	$G_e, \{g_k\}_{k=1}^N$	$\{g_k\}_{k=1}^N$
G_e	$1/J_e$	
g_k	$\left(-J_e + \sum_{i=1}^N \frac{j_i\alpha_k^2}{(\beta_i-\alpha_k)^2}\right)^{-1}$	$\left(-J_e + \frac{2\eta_0^{-1}}{\alpha_k} + \sum_{i=1}^{N-1} \frac{j_i\alpha_k^2}{(\beta_i-\alpha_k)^2}\right)^{-1}$

TABLE II. Explicit expressions for parameters and coefficients of the target Prony series.

situation can be illustrated using a single mode viscoelastic liquid,

$$\tilde{J}(s) = \frac{J_e}{s} + \frac{\eta_0^{-1}}{s^2} - \frac{j_1}{s+\beta_1} = \frac{s^2(J_e - j_1) + s(J_e\beta_1 + \eta_0^{-1}) + \beta_1\eta_0^{-1}}{s^2(s+\beta_1)}. \tag{10}$$

From Table II or the quadratic form of the numerator, we expect $\tilde{J}(s)$ to have two zeros $-\alpha_1$ and $-\alpha_2$ such that $\infty > \alpha_1 > \beta_1 > \alpha_2 > 0$. However, when $J_e = j_1$, the s^2 term in the numerator becomes zero, and we are left with a single root.

In experiments, this corner case is moot because direct measurement of $J(0)$ requires application of an instantaneous step stress. This is an idealization that is impossible to realize in practice. Nevertheless, this corner case helps to illuminate the most important algorithmic difference between PSI and LdHA which relates to how the roots of the Laplace transform of the source function are determined. The LdHA paper mentions that for $J \to G$ interconversion, the poles of $\tilde{J}(s)$ where the function becomes singular interferes with accurately determining the roots (section

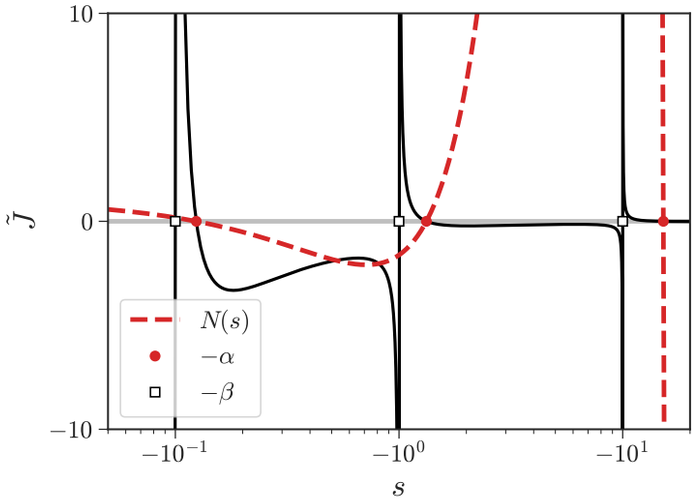

FIG. 1. The Laplace transform $\tilde{J}(s)$ for a viscoelastic solid with 3 retardation modes indicated by the poles (open squares). The dashed red line denotes the numerator $N(s)$ when $\tilde{J}(s) = N(s)/D(s)$ is expressed as a ratio of two polynomials. The roots of $N(s)$ coincide with the roots of $\tilde{J}(s)$ and are indicated by red circles.

"Numerical aspects of determining the zeros" of reference 31).

In PSI, rather than finding the roots of $\tilde{J}(s)$ directly, we express it as a ratio of two polynomials $\tilde{J}(s) = N(s)/D(s)$, similar to the last expression in equation 10. In python, this operation can be numerically implemented using the function `invres` from the standard module for signal processing (`scipy.signal`). The roots of $\tilde{J}(s)$ are determined solely by $N(s)$. Hence we solve $N(s) = 0$ to determine the roots, without any interference from the poles which are consigned to the denominator $D(s)$. We believe that LdHA were aware of this trick since they remark at one point: "The numerical aspects are reduced to finding the zeros of certain polynomials, for which there is a plethora of sources" [31].

The power of this tactic is demonstrated in figure 1 for a viscoelastic solid with $J_e = 1$, and $N = 3$ retardation modes $j_1 = j_2 = j_3 = 0.2$ and $\lambda_1 = 0.1$, $\lambda_2 = 1$, and $\lambda_3 = 10$. The Laplace transform $\tilde{J}(s) = J_e/s + \sum_{k=1}^{3} j_k(s+\beta_k)^{-1}$ is shown by the solid black line. It has nonzero poles at $-\beta_1 = -10$, $-\beta_2 = -1$, and $-\beta_3 = -0.1$, which are marked by open squares. $\tilde{J}(s)$ diverges and changes signs at these points. The roots of $\tilde{J}(s)$ occur at $-\alpha_1 \approx -15.2$, $-\alpha_2 \approx -1.33$, and $-\alpha_3 \approx -0.12$, and are shown by the solid red circles. From visual inspection, we find that the

roots and poles of $\tilde{J}(s)$ obey the interlacing property (equation 8),

$$\alpha_1 > \beta_1 > \alpha_2 > \beta_2 > \alpha_3 > \beta_3.$$

We can express $\tilde{J}(s) = N(s)/D(s)$ as a ratio of two polynomials. The numerator $N(s)$ is a smooth cubic polynomial, depicted by the dashed red line. It shares the same roots as $\tilde{J}(s)$, but is much smoother since it is free from singularities. Thus, numerically, it is much easier to find the roots of the polynomial $N(s)$ than the rational function $\tilde{J}(s)$.

While it is easier to find the roots of $\tilde{G}(s)$ compared to $\tilde{J}(s)$, we adopt the same method of expressing $\tilde{G}(s)$ as a ratio of two polynomials and finding the zeros of the numerator to determine the roots of $\tilde{G}(s)$. Furthermore, for parsimonious spectra with 10 – 20 discrete modes used to describe the majority of experimental and simulation data, we find that the built-in python function `numpy.roots` works remarkably well. This method to find the roots relies on computing the eigenvalues of the companion matrix [41], and does not exploit the interlacing property.

B. Test Problems

We test the computer program PSI on several example problems. They include several problems for which analytical or prior numerical solutions are available. We test the conversion for both $G \to J$ and $J \to G$.

1. **Viscoelastic solid and liquid with a single Maxwell mode**

   For a solid, the relaxation modulus takes the form,

   $$G(t) = G_e + g_1 \exp(-t/\tau_1), \tag{11}$$

   with $G_e = 1$ Pa, $g_1 = 10$ Pa and $\tau_1 = 10$ s. This serves as a useful test to verify PSI because the analytical form for the corresponding creep compliance is known. It is given by,

   $$J(t) = J_e - j_1 \exp(-t/\lambda_1), \tag{12}$$

   with $J_e = 1/G_e$, $j_1 = G_e^{-1} - (G_e + g_1)^{-1}$, and $\lambda_1 = \tau(1 + g_1/G_e)$.

   A single mode viscoelastic liquid takes the form,

   $$G(t) = g_1 \exp(-t/\tau_1). \tag{13}$$

We set $g_1 = 10$ Pa and $\tau_1 = 10$ s, as before. Since $N - 1 = 0$, the compliance does not contain any retardation times, and instead takes the form,

$$J(t) = \frac{1}{g_1} + \frac{t}{g_1 \tau_1}. \tag{14}$$

2. **Tensile Relaxation Modulus**

We consider a "classic" dataset on the tensile relaxation modulus of polymethyl methacrylate (PMMA) whose Prony series representation has previously been used in numerous studies on interconversion [26, 27, 31, 42]. The experimental data extends over 10 orders of magnitude, and uses a discrete relaxation spectrum with 11 modes that are spaced one decade apart. This is reproduced in supplementary material in the section "Prony series data".

The data are results of a tensile test; nevertheless, we use the symbol $G(t)$ which is reserved for shear relaxation modulus to avoid introducing new nomenclature. Since the focus of this work is interconversion between relaxation modulus and compliance, the nature of the test (tensile or shear) is not particularly important.

Although the system is non-crosslinked, it exhibits an entanglement plateau modulus which is assumed to be equal to G_e in the Prony series representation in all previous analysis of this dataset. Technically, this treats the material as a viscoelastic solid, even though a terminal plateau is not visible in the raw data. For ease of comparison, we adopt the same outlook. In other words, our starting point is the Prony series for the relaxation modulus presented to describe the original experimental data [27].

3. **Ring polymer relaxation modulus**

This data set is obtained from stress relaxation data on non-catenated polystyrene ring polymer melts of molecular weight 198 kDa [43]. The material is a viscoelastic liquid, and hence has $G_e = 0$. $G(t)$ exhibits an apparent power law behavior over four decades of time, before a faster relaxation process takes over.

The discrete relaxation spectrum for this dataset was computed using the computer program pyReSpect-time, previously developed in our group, and was reported as figure 7 in reference 37. It yields an 8 mode discrete relaxation spectrum which is also presented as supplementary material.

4. **Compliance of an Asphalt mixture**

The rheology of asphalt mixtures is important for road and pavement design. Experimentally, it is much more convenient to measure $J(t)$ rather than $G(t)$. However, conversion of the $J(t)$ data to $G(t)$ is often sought for incorporation into finite element analysis software. Unlike experimental data on PMMA or ring polymers discussed above, this test considers $J \to G$ interconversion.

We use the compliance data on hot mix asphalt AC-13 with performance grade binder PG70-22. $J(t)$ is collected over multiple temperatures to create a mastercurve that spans over 8 decades of timescales [10]. The authors of the original study use two different methods to obtain $G(t)$, but assume that the retardation times are the same as the relaxation times ($\lambda_k = \tau_k$). The Prony series representation of the $J(t)$ data, and the converted $G(t)$ (using a least squares approach) are presented as supplementary material. This offers an interesting test case to see if using a different method results in a substantially different $G(t)$.

5. Compliance and Dynamic Modulus of Monodisperse Polyisoprene

Finally, we consider experimental data on a nearly monodisperse (polydispersity index of 1.03) polyisoprene (PI) polymer with weight-averaged molecular weight of 152 kg/mol. Both creep compliance $J(t)$ and dynamic modulus $G^*(\omega)$ are reported over a comparable range of timescales for this sample [44]. This study also reported an elegant non-parametric method for direct numerical conversion of $J(t) \to G^*(\omega)$. In this work, we label this procedure as “Evans method". An important use case for this method is microrheology [45], where $J(t)$ is proportional to the measured mean-squared displacement $\langle \Delta r^2(t) \rangle$ of tracer particles with radius a, $J(t) = (\pi a / k_B T) \langle \Delta r^2(t) \rangle$, and conversion to $G^*(\omega)$ is desired.

Evans method can directly be applied to raw creep compliance data (see figure S1 in supplementary material). However, to investigate the propagation of experimental noise, they also fitted their observations to a purely empirical smooth curve given by,

$$J(t) = \frac{t}{\eta_0} + a + b \tanh\left(c + d \log t + e(\log t)^2 + f(\log t)^3\right) \tag{15}$$

with fitting parameters $\eta_0 = 1.1453$ MPa·s, $a = 4.7 \times 10^{-6}$ Pa^{-1}, $b = 2.4 \times 10^{-6}$ Pa^{-1}, $c = 0.288082$, $d = 0.247501$, $e = 0.0174205$, and $f = 0.000685812$ [44]. This implies $J(0) = 2.3 \times 10^{-6}$ Pa^{-1}.

PSI can also be used for $J(t) \to G^*(\omega)$ interconversion by first fitting a Prony series representation to the raw $J(t)$ data. We force J_e and η_0^{-1} to be consistent with the parameters $J(0)$

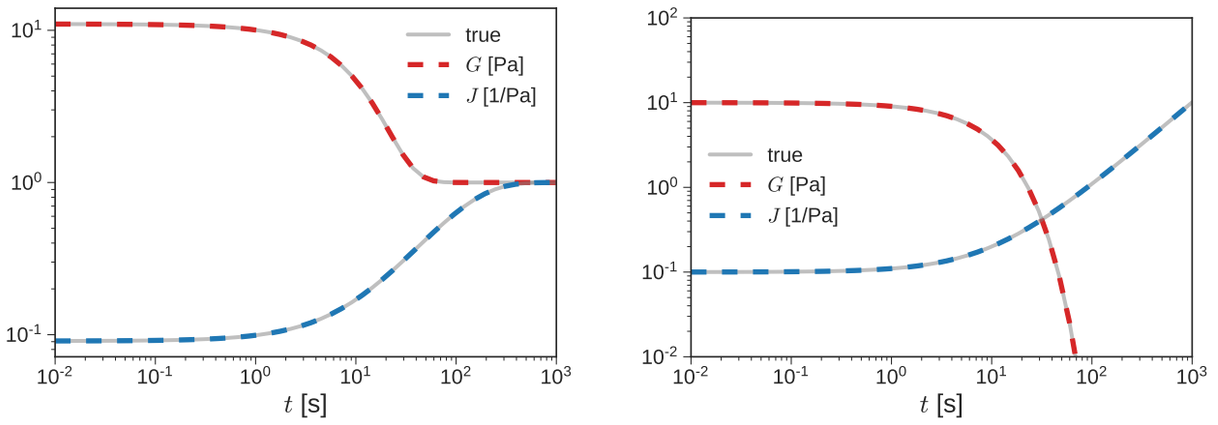

(a) viscoelastic solid

(b) viscoelastic liquid

FIG. 2. **Single mode Maxwell model**: The true (gray lines) and inferred (dashed lines) LVE functions for a viscoelastic (a) solid, and (b) liquid. The inferred moduli (red) and compliances (blue) overlap with the true LVE functions.

and η_0 used in equation 15. We then fit a discrete retardation spectrum with three modes which is presented in the supplementary material (Table S4).

We then use PSI to obtain a discrete relaxation spectrum $\{g_k, \tau_k\}$ from this retardation spectrum. In general, the storage ($G'(\omega)$) and loss ($G''(\omega)$) moduli, where $G^*(\omega) = G'(\omega) + iG''(\omega)$, can be calculated from the discrete relaxation spectrum using,

$$G'(\omega) = \sum_k \frac{g_k \omega^2 \tau_k^2}{1+\omega^2\tau_k^2} + G_e$$
$$G''(\omega) = \sum_k \frac{g_k \omega \tau_k}{1+\omega^2\tau_k^2}. \tag{16}$$

Here $G_e = 0$, since the PI polymer is a viscoelastic liquid.

III. RESULTS

Figure 2 graphically compares the true and interconverted $G(t)$ and $J(t)$ for the single mode Maxwell test problem. For the viscoelastic solid with $G_e = 1$ Pa, $g_1 = 10$ Pa and $\tau_1 = 10$ s (equation 11), PSI correctly predicts $J_e = 1$ Pa^{-1}, $j_1 = 10/11$ Pa^{-1}, and $\lambda_1 = 110$ s, when we use it for $G \to J$ conversion. Using these inferred values and performing a $J \to G$ conversion using

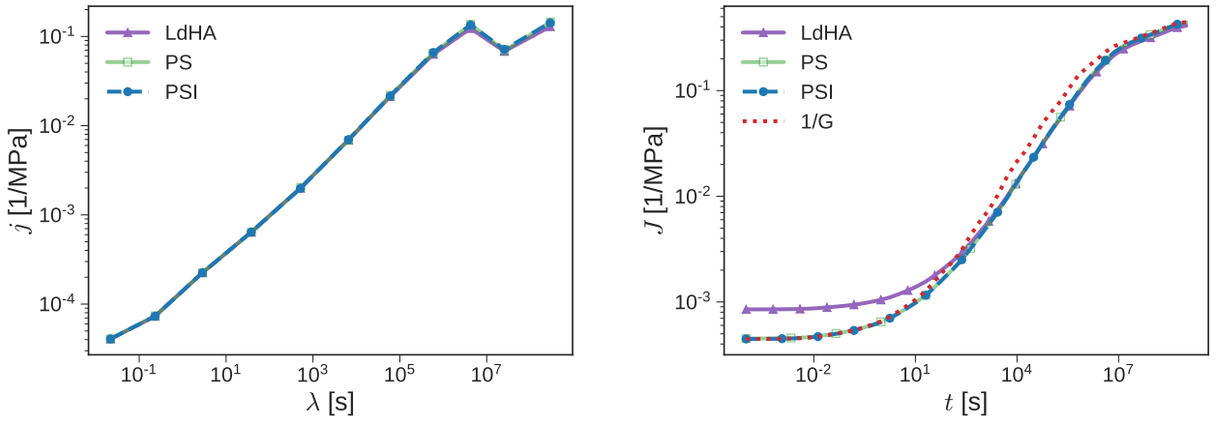

(a) retardation spectrum

(b) creep compliance

FIG. 3. **PMMA**: Comparison of (a) retardation spectrum, and (b) creep compliance for a PMMA sample [42]. PS and LdHA represent interconversions for this classic dataset reported by Park and Schapery [27], and Loy et al. [31], respectively. The retardation spectra obtained using the different methods essentially overlap. The creep compliance shows some disagreement at short times due to uncertainty in the value of J_e used in LdHA.

PSI returns the original parameters, as expected. For the viscoelastic liquid (equation 13), PSI correctly predicts $J_e = 0.1$ Pa^{-1}, and $\eta_0^{-1} = 0.01$ Pa·s.

We also tested PSI on the single mode Maxwell model with numerically different values for the Prony series parameters. In all cases, PSI successfully returned the expected analytical values for the converted LVE function. This test problem serves as a useful verification problem, since the analytical solution can be used as a benchmark. The observation that applying $G \to J$ and $J \to G$ transformations in succession returns the originally used Prony series parameters is also a useful test, and highlights the consistency of PSI.

Figure 3a compares the spectra inferred using PSI with previous work on the PMMA tensile relaxation data [42]. PS and LdHA are spectra inferred for this classic problem by Park and Schapery [27], and Loy et al. [31], respectively. All three spectra show remarkable agreement. We observe that the shape of the spectrum inferred using PSI is relatively more aligned with PS than with LdHA, especially at long retardation times. This is mildly surprising since PSI and LdHA effectively share the same algorithm, while Park and Schapery use a least squares approach that requires solving a linear algebraic system. Indeed, we find that the locations of the retardation

times for PSI and LdHA are identical, and slightly different from PS. However, the coefficients $\{j_k\}$ are not the same.

The source of the discrepancy may simply be a typographical error. Alternatively, it may stem from the value of G_e used in LdHA, which differs from the original data [27, 42], where $G_e = 2.24$ MPa. Using the LdHA method or PSI, this should yield $J_e = 1/G_e = 0.4464$ MPa^{-1}. Instead, LdHA report $J_e = 0.41525$ MPa^{-1} [31]. This is evident in figure 3b, which shows $J(t)$ corresponding to the different spectra in figure 3a, along with the reciprocal of the relaxation modulus. From the convolution relation (equation 5), at short times $J(t) \approx 1/G(t)$. It can be seen that PS and PSI essentially overlap and superpose with $1/G(t)$ at short times as expected. However, LdHA overestimates $J(t)$ in this limit. The difference between the methods can be fixed by adjusting the value of J_e used in LdHA.

Figure 4a compares the inferred creep compliance with the inverse of the relaxation modulus obtained from experiments for ring polymers. The first thing we observe is that they are of comparable magnitude: for quasielastic materials we expect $J(t) = 1/G(t)$. For weakly viscoelastic materials, other empirical approximations have been proposed [27].

In the figure, $J(t)$ and $1/G(t)$ exhibit an apparent power-law behavior over several decades. This is indicated by the gray line which denotes the power-law $t^{0.45}$. The power-law dependence is also observed in the discrete spectra shown in figure 4b, where the inverse of the coefficients $\{g_k\}$ are shown for ease of comparison with the coefficients $\{j_k\}$. The gray line in this subfigure also follows the same power-law.

For materials like critical gels which exhibit a single power-law exponent m, $J(t)$ and $G(t)$ are related via $G(t)J(t) = \sin(m\pi)/(m\pi)$. Based on this exact relation, numerous approximate relationships between $J(t)$ and $G(t)$ have been proposed over the years for materials that exhibit approximate power-law behavior [2, 46]. These approximations are expected to work well when source function ($G(t)$ in this case) is characterized by smooth behavior on a double logarithmic plot.

Here, we consider four such relations, and evaluate how they fare for this test problem [46]. All these relations use a local power-law exponent $m(t) = |d\log G(t)/d\log t|$. The first approximation, given by Leaderman [47], replaces the constant exponent with the local exponent. Hence,

$$G(t)J(t) \approx \frac{\sin m(t)\pi}{m(t)\pi}. \tag{17}$$

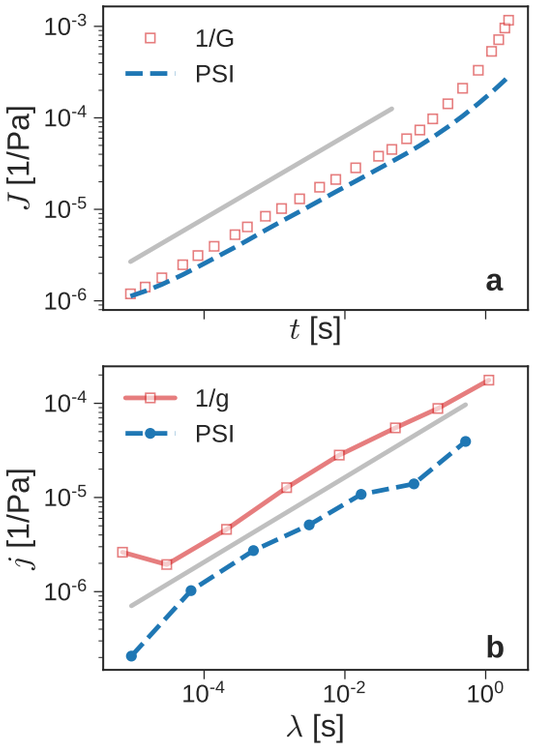

FIG. 4. **Ring polymer**: (a) creep compliance (dashed blue line) is compared to the reciprocal of the experimental relaxation modulus (open squares). Both LVE functions exhibit an apparent power-law behavior $t^{0.45}$ depicted by the gray line. (b) the inferred retardation spectrum (blue circles joined by dashed lines), and the inverse of the coefficients of the relaxation spectrum also exhibit a similar power-law behavior as shown by the gray line.

Another version due to Denby [48] offers,

$$G(t)J(t) \approx \frac{1}{1+(\pi^2/6)\,m^2(t)}. \tag{18}$$

A similar approximation by Christiansen proposes, [49],

$$G(t)J(t) \approx \frac{1}{1+(\pi^2/4)\,m^2(t)}. \tag{19}$$

Finally, Park and Kim [46] suggest $J(t) = 1/G(\alpha t)$ where,

$$\alpha = \left(\frac{\sin m(t)\pi}{m(t)\pi}\right)^{1/m(t)} \tag{20}$$

can be interpreted as shift factor along the logarithmic time coordinate.

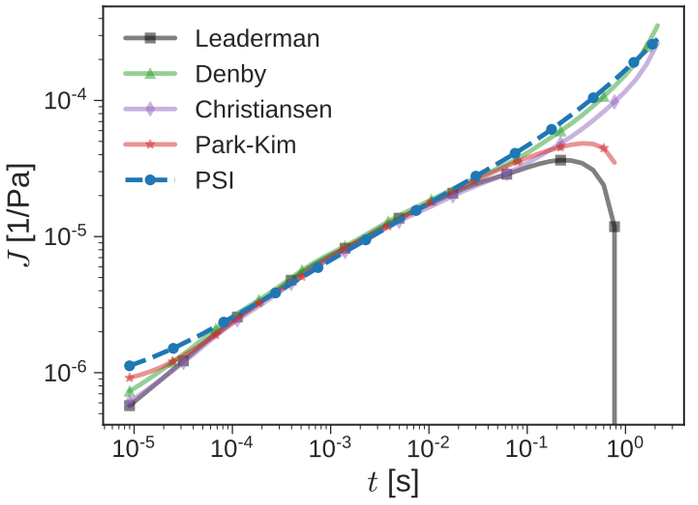

FIG. 5. **Ring polymer**: Creep compliance inferred using PSI (blue circles connected by dashed line) is compared with different approximate relations for direct interconversion of $G(t)$ to $J(t)$ given by equations 17 - 20.

The predictions of these approximate expressions are shown in figure 5. Over a broad range of intermediate timescales ($10^{-4} - 10^{-1}$ s), all these approximations yield predictions that are nearly indistinguishable from that of PSI. At shorter timescales, these approximations underpredict $J(t)$. The relationship proposed by Park and Kim offers the closest approximation in this regime. At longer times, the relationship proposed by Denby offers the closest approximation, followed by that of Christiansen. The other two approximations diverge due to the presence of the sine term. This shows both the utility and danger of using approximate relations: they provide good estimates when the source function is smooth, but the nature and magnitude of the error is difficult to anticipate. The goal of PSI is to provide a convenient tool for interconversion; this might help uncontrolled approximate interconversions from being used during data analysis.

Figure 6 considers $J \to G$ interconversion for an experimental dataset on mixed asphalt. We observe that $G \approx 1/J$ which may be expected for a quasi-elastic material. The solid black line is the prediction for the modulus using the spectrum obtained by Zhang et al. [10], and is hence labeled as "Z18". It is indistinguishable from the prediction of $G(t)$ using PSI, which is shown by the dashed red line.

Zhang et al. obtained the discrete relaxation spectrum shown in figure 6b by placing a uniform grid of relaxation times $\{\tau_k\}$ on a logarithmic scale, and inferring the coefficients $\{g_k\}$ using a

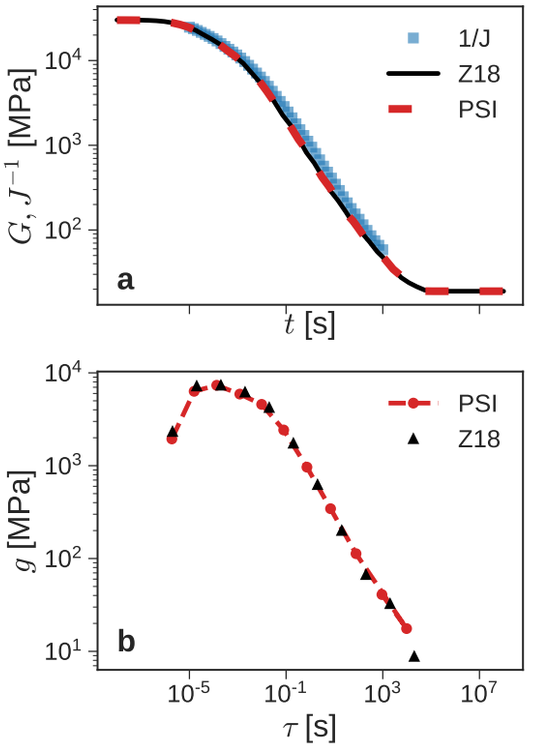

FIG. 6. **Asphalt mixture**: (a) relaxation moduli obtained using PSI (dashed red line) and by Zhang et al. [10] (black line) are compared with the inverse of the experimental creep compliance (open blue squares). (b) the shapes of the relaxation spectra inferred by PSI (circles joined by dashed line) and Zhang et al. [10] (black triangles) are similar.

least squares procedure. On the other hand, the discrete relaxation times obtained by PSI are not uniformly spaced, and are the zeros of $\tilde{J}(s)$. Nevertheless the shapes of the spectra are quite similar, and they lead to predictions of $G(t)$ that are essentially identical. This illustrates another useful point: the discrete spectra are not unique, and similar spectra often lead to LVE functions that are indistinguishable. While the shape of the discrete spectrum is still meaningful, it is also an important reminder not to overinterpret the inferred spectrum [1, 12, 50, 51].

In the final test problem, experimental data are available for both compliance and dynamic moduli which allow us to compare interconverted viscoelastic functions with experiments. Here, we focus on $J(t) \to G^*(\omega)$, and use both Evans method and PSI for interconversion. Evans method is a simple and elegant method takes creep compliance tabulated as N discrete data points $\{(t_1, J_1), \cdots, (t_N, J_N)\}$, where $J_k = J(t_k)$. The spacing between successive time intervals can be

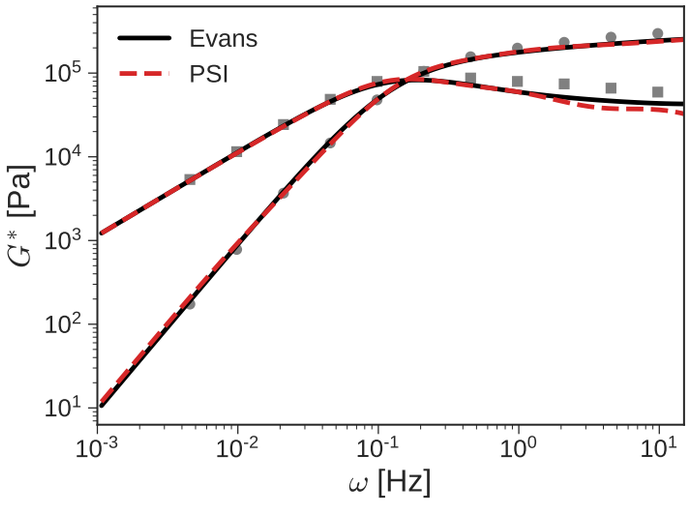

FIG. 7. **Monodisperse PI**: Gray symbols denote experimentally measured storage (circles) and loss (squares) moduli. The solid black lines show $J \rightarrow G^*$ interconversion via Evans method (equation 21) using a smooth fit to experimental data (equation 15). The dashed red lines show $J \rightarrow G^*$ interconversion using PSI and equation 16.

non-uniform. It also requires two additional parameters $J(0)$ and η_0 which can be obtained by fitting or extrapolating experimental data. Then, $G^*(\omega) = G'(\omega) + iG''(\omega)$ is given by the relation

$$\frac{i\omega}{G^*(\omega)} = i\omega J(0) + \left(1 - e^{-i\omega t_1}\right)\frac{J_1 - J(0)}{t_1} + \frac{e^{-i\omega t_1}}{\eta_0} + \sum_{k=2}^{N}\left(\frac{J_k - J_{k-1}}{t_k - t_{k-1}}\right)\left(e^{-i\omega t_{k-1}} - e^{-i\omega t_k}\right) \quad (21)$$

Figure 7 shows the comparison between the experimentally measured dynamic modulus (symbols), and the $G^*(\omega)$ obtained using Evans method (solid black lines) with $N = 200$ logarithmically equispaced points $\{t_k\}$ between 10^{-2} and 10^3 s. The corresponding $\{J_k\}$ are obtained from the smooth empirical fit (equation 15) to the raw data. The interconverted dynamic moduli show excellent agreement with experimental data at low frequency. However, $G'(\omega)$ and $G''(\omega)$ are underestimated at high frequencies [44]. This discrepancy is attributed to "starting transients in the creep data or imperfect equilibration since miscalibration, nonlinearities, edge fracture, and other possible sources have been exhaustively eliminated."

Using the Prony series representation (Table S4 in supplementary material) of the experimental creep compliance data, we use PSI to obtain $\{g_k, \tau_k\}$ from $\{j_k, \lambda_k\}$. The storage and loss moduli are subsequently calculated using equation 16. These results are shown by dashed red lines in figure 7: they are comparable with the predictions using Evans method. This example highlights

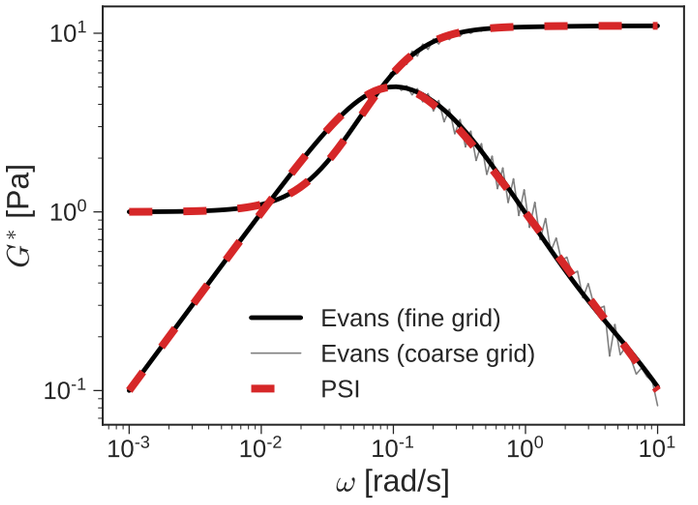

FIG. 8. **Single mode viscoelastic solid**: Dynamic moduli are calculated from noise-free $J(t)$ corresponding to the single mode Maxwell solid considered earlier in figure 2. Interconversion using PSI (dashed red lines) and Evans method corresponding to densely distributed input data (solid black lines) yield similar results. However, when the temporal spacing is increased (thin gray lines) we observe spurious fluctuations.

several strengths of Evans method, viz. (i) it allows for direct numerical calculation, (ii) it can deal with both raw or smoothed input data, and (iii) it is remarkably easy to implement once $J(0)$ and η_0 are estimated.

However, like all numerical algorithms, Evans method has its share of drawbacks. Perhaps the most serious limitation is its susceptibility to discretization error that arises from approximating derivatives using finite differences. It is well-known from numerical analysis that finite difference approximations magnify fluctuations in input data [19]. We reconsider the example of a single mode viscoelastic solid (previously shown in figure 2a) to illustrate the susceptibility of Evans method to discretization error in figure 8. We first employ a fine temporal grid using $N = 100$ logarithmically equispaced points between 0.1 and 1000 s. We use equation 12 to generate noiseless synthetic compliance data at these grid points. We set the parameters $J(0) = 1/11$ and $\eta_0 = \infty$ to theoretically exact values. The solid black lines in figure 8 show the results of Evans method for this fine grid. These predictions are similar to the theoretically exact $G^*(\omega)$ obtained using PSI shown by the dashed red lines.

We then generate synthetic data on a coarser temporal grid by using half as many points ($N =$

50) over the same time window. When Evans method is used to obtain $G^*(\omega)$, we observe spurious fluctuations at high frequencies that are especially serious for $G''(\omega)$. Note that this error is purely numerical since the input data are noiseless (strictly, the level of noise, $\mathcal{O}(10^{-16})$, is determined by machine precision).

IV. DISCUSSION

In this section, we discuss the speed and reliability of PSI. In terms of speed, PSI is extremely fast: all reported calculations required 10 ms or less on a Linux desktop computer with an Intel i7-6700 3.40GHz CPU. Practically, interconversion using PSI is instantaneous; a more detailed analysis of computational cost is unnecessary. This speed opens up future lines of inquiry. For example, it can be exploited for uncertainty quantification of the target signal by propagating uncertainties in the parameters of the Prony series representation of the source signal using Monte Carlo simulations. Furthermore, it may be possible to combine experimental measurements of compliance and modulus by using PSI as an intermediate step to jointly infer the relaxation and retardation spectra.

A. Limitations of PSI

We performed extensive testing to identify the boundary beyond which PSI fails due to numerical issues. The format of these tests used the following protocol:

1. Select an odd number of modes $N = 2n+1$, with relaxation times that are spaced one decade apart. Assume that the coefficients of the Prony series are constant. That is, for $k = 1, \cdots N$, $\tau_k = 10^{k-n-1}$ and $g_k = 1/N$. For example, when n = 2 (N = 5 modes), the relaxation times are $10^{\pm 2}$, $10^{\pm 1}$, and 10^0, and the coefficients are all equal to $1/N = 0.2$.

2. Perform $G \rightarrow J$ interconversion to find the Prony series corresponding to $J(t)$

3. Perform $J \rightarrow G$ interconversion, using the Prony series computed in the step above

4. Compare the resulting Prony series with the original input. Check if they are identical. Monitor any problems encountered during the calculation.

Let us define the span of the input data D_{span} as the number of decades spanned by the relaxation time constants,

$$D_{\text{span}} = \log_{10}(\tau_N/\tau_1). \tag{22}$$

For typical values of D_{span} encountered in experimental or computational data, PSI is consistent and fast, as previously observed for test problems. However, for $D_{\text{span}} \approx 24$, PSI starts to suffer from numerical issues. The root-finding step of the method begins yielding complex numbers, which causes downstream problems that interfere with determining the coefficients of the target Prony series. Using bisection with the interlacing property also runs into analogous difficulties.

We experimented with different spacing of relaxation times, e.g. $\tau_k = 2^{k-n-1}$ instead of $\tau_k = 10^{k-n-1}$, and found that PSI failed at different values of N, all of which corresponded to $D_{\text{span}} \approx 24$. Thus, it is not the number of modes N, but the range of the discrete spectrum D_{span} that controls success or failure of PSI.

The location of the failure is insensitive to the nature of the material. We added a plateau modulus ($G_e = 1$) to the protocol mentioned above to consider a viscoelastic solid, instead of a viscoelastic liquid. Nevertheless, numerical issues still surfaced only around $D_{\text{span}} \approx 24$. Furthermore, we also explored sampling the coefficients g_k randomly from the interval $[0.01, 1/N]$. The threshold for numerical stability remained essentially unchanged. In summary, we find that PSI is numerically stable for datasets that span less than 24 decades of time. Fortunately, this is large enough to include most computational and experimental data.

V. CONCLUSIONS

Interconversion of $G(t)$ and $J(t)$ is an important problem in linear rheology. Despite the abundance of numerical methods proposed to solve the problem, most published studies have not been distributed as software programs. This work describes an open-source Python program called PSI which is free and easy to use. It can be used for both $G \to J$ and $J \to G$ interconversions. PSI takes a parsimonious Prony series representation of the source LVE function as input, and calculates the Prony series corresponding to the target LVE function as output.

It relies on the two-step method developed by LdHA in which time constants and coefficients of the Prony series are computed one after the other. Small mathematical modifications to the LdHA algorithm noted in section II side step singularities, and stabilize the root-finding exercise.

We tested PSI on a variety of materials including viscoelastic solids and liquids. Applying

$G \to J$ and $J \to G$ interconversions in sequence yielded the original input data, demonstrating its consistency. Practically, numerical instability was found to be insignificant, unless the input discrete spectrum spanned over twenty decades. The origin of this unexpected stability is possibly the natural regularization provided by a parsimonious input spectrum, and the mathematical trick employed to bypass poles of the Laplace transform. Unlike approximate methods of interconversion, PSI does not place any additional assumptions on the shapes of the source LVE functions. It fills an important gap in the existing software landscape for conversion of LVE functions, and is expected to be useful to experimental rheologists.

SUPPLEMENTARY MATERIAL

Please see supplementary material for (i) links to software for computing discrete relaxation and retardation spectra, (ii) Prony series data used as input to PSI for the test examples, and (iii) a short tutorial for using PSI.

ACKNOWLEDGMENTS

We acknowledge support from the Department of Scientific Computing at Florida State University, and Prof. Ralm G. Ricarte for motivating this work.

DATA AVAILABILITY STATEMENT

The Python code for PSI is freely available at `https://github.com/shane5ul/psi`. Other data that support the findings of this study are available from the corresponding author upon reasonable request.

[1] J. D. Ferry, *Viscoelastic properties of polymers*, 3rd ed. (John Wiley & Sons, New York, NY, 1980).

[2] N. W. Tschoegl, *The phenomenological theory of linear viscoelastic behavior: An introduction*, 1st ed. (Springer-Verlag, Munich, Germany, 1989).

[3] D. J. Plazek and I. Echeverria, Don't cry for me Charlie Brown, or with compliance comes comprehension, J. Rheol. **44**, 831 (2000).

[4] S. J. Park, S. Shanbhag, and R. G. Larson, A hierarchical algorithm for predicting the linear viscoelastic properties of polymer melts with long-chain branching, Rheol. Acta **44**, 318 (2005).

[5] C. Das, N. J. Inkson, D. J. Read, M. A. Kelmanson, and T. C. B. McLeish, Computational linear rheology of general branch-on-branch polymers, J. Rheol. **50**, 207 (2006).

[6] D. J. Read, D. Auhl, C. Das, J. den Doelder, M. Kapnistos, I. Vittorias, and T. C. B. McLeish, Linking models of polymerization and dynamics to predict branched polymer structure and flow, Science **333**, 1871 (2011).

[7] S. Shanbhag, Fast slip link model for bidisperse linear polymer melts, Macromolecules **52**, 3092 (2019).

[8] S. Shanbhag, Mathematical foundations of an ultra coarse-grained slip link model, J. Chem. Phys. **151**, 044903 (2019).

[9] Y. R. Kim, *Modeling of asphalt concrete* (McGraw-Hill Education, Raleigh, NC, USA, 2009).

[10] W. Zhang, B. Cui, X. Gu, and Q. Dong, Comparison of relaxation modulus converted from frequency- and time-dependent viscoelastic functions through numerical methods, Appl. Sci. **8**, 10.3390/app8122447 (2018).

[11] S. Mun, G. R. Chehab, and Y. R. Kim, Determination of time-domain viscoelastic functions using optimized interconversion techniques, Road Mater. Pavement Des. **8**, 351 (2007).

[12] K. S. Cho, *Viscoelasticity of Polymers: Theory and Numerical Algorithms* (Springer, Dordrecht, the Netherlands, 2016).

[13] C. T. Baker, A perspective on the numerical treatment of Volterra equations, J. Comput. Appl. Math. **125**, 217 (2000).

[14] I. L. Hopkins and R. W. Hamming, On creep and relaxation, J. Appl. Phys. **28**, 906 (1957).

[15] W. F. Knoff and I. L. Hopkins, An improved numerical interconversion for creep compliance and relaxation modulus, J. Appl. Polym. Sci. **16**, 2963 (1972).

[16] P. Linz, *Analytical and Numerical Methods for Volterra Equations* (SIAM, Philadelphia, 1985).

[17] A. Nikonov, A. R. Davies, and I. Emri, The determination of creep and relaxation functions from a single experiment, J. Rheol. **49**, 1193 (2005).

[18] J. Sorvari and M. Malinen, Numerical interconversion between linear viscoelastic material functions with regularization, Int. J. Solids Struct. **44**, 1291 (2007).

[19] M. Heath, *Scientific Computing: An Introductory Survey*, 2nd ed. (McGraw-Hill, 2002).

[20] D. W. Mead, Numerical interconversion of linear viscoelastic material functions, J. Rheol. **38**, 1769 (1994).

[21] F. R. de Hoog, J. H. Knight, and A. N. Stokes, An improved method for numerical inversion of Laplace transforms, SIAM J. Sci. Comput. **3**, 357 (1982).

[22] A. M. Cohen, *Numerical Methods for Laplace Transform Inversion*, 1st ed. (Springer Publishing Company, Incorporated, 2007).

[23] G. R. de Prony, Essai experimental et analytique: sur les lois de la dilatabilite des fluides elastique et sur celles de la force expansive de la vapeur de l'eau et de la vapeur de l'alkool, a differentes temperatures, J. Ecole Poly. **1**, 24 (1795).

[24] B. Gross, *Mathematical Structure of the Theories of Viscoelasticity* (Hermann, Paris, 1953).

[25] M. Baumgaertel and H. H. Winter, Determination of discrete relaxation and retardation time spectra from dynamic mechanical data, Rheol. Acta **28**, 511 (1989).

[26] J. Sorvari and M. Malinen, On the direct estimation of creep and relaxation functions, Mech. Time-Depend. Mater. **11**, 143 (2007).

[27] S. Park and R. Schapery, Methods of interconversion between linear viscoelastic material functions. Part I - a numerical method based on Prony series, Int. J. Solids Struct. **36**, 1653 (1999).

[28] J. Luk-Cyr, T. Crochon, C. Li, and M. Lévesque, Interconversion of linearly viscoelastic material functions expressed as Prony series: a closure, Mech. Time-Depend. Mater. **17**, 53 (2013).

[29] Y. Liu, A direct method for obtaining discrete relaxation spectra from creep data, Rheol. Acta **40**, 256 (2001).

[30] P. J. Dooling, C. P. Buckley, and S. Hinduja, An intermediate model method for obtaining a discrete relaxation spectrum from creep data, Rheol. Acta **36**, 472 (1997).

[31] R. J. Loy, F. R. de Hoog, and R. S. Anderssen, Interconversion of Prony series for relaxation and creep, J. Rheol. **59**, 1261 (2015).

[32] E. T. Whittaker, On the numerical solution of integral-equations, Proc. Roy. Soc. A **94**, 367 (1918).

[33] R. S. Anderssen, A. R. Davies, and F. R. de Hoog, On the Volterra integral equation relating creep and relaxation, Inverse Prob. **24**, 035009 (2008).

[34] R. S. Anderssen, A. R. Davies, and F. R. de Hoog, On the sensitivity of interconversion between relaxation and creep, Rheol. Acta **47**, 159 (2008).

[35] R. S. Anderssen, A. R. Davies, and F. R. de Hoog, On the interconversion integral equation for relaxation and creep, ANZIAM J. **48**, C346 (2007).

[36] A. Takeh and S. Shanbhag, A computer program to extract the continuous and discrete relaxation spectra from dynamic viscoelastic measurements, Appl. Rheol. **23**, 24628 (2013).

[37] S. Shanbhag, pyReSpect: A computer program to extract discrete and continuous spectra from stress relaxation experiments, Macromol. Theory Simul. , 1900005 (2019).

[38] S. Shanbhag, Relaxation spectra using nonlinear Tikhonov regularization with a Bayesian criterion, Rheol. Acta **59**, 509 (2020).

[39] S. W. Provencher, An eigenfunction expansion method for the analysis of exponential decay curves, J. Chem. Phys. **64**, 2772 (1976).

[40] K. Suman, S. Shanbhag, and Y. M. Joshi, Phenomenological model of viscoelasticity for systems undergoing sol-gel transition, Phys. Fluids **33**, 10.1063/5.0038830 (2021).

[41] R. A. Horn and C. R. Johnson, *Matrix Analysis* (Cambridge University Press, 1990).

[42] R. A. Schapery, *A simple collocation method for fitting viscoelastic models to experimental data*, Tech. Rep. GALCIT SM 61-23A (California Institute of Technology, Pasadena, CA, 1962).

[43] M. Kapnistos, M. Lang, D. Vlassopoulos, W. Pyckhout-Hintzen, D. Richter, D. Cho, T. Chang, and M. Rubinstein, Unexpected power-law stress relaxation of entangled ring polymers, Nat. Mater. **7**, 997 (2008).

[44] R. M. L. Evans, M. Tassieri, D. Auhl, and T. A. Waigh, Direct conversion of rheological compliance measurements into storage and loss moduli, Phys. Rev. E **80**, 012501 (2009).

[45] M. Tassieri, R. M. L. Evans, R. L. Warren, N. J. Bailey, and J. M. Cooper, Microrheology with optical tweezers: data analysis, New J. Phys. **14**, 115032 (2012).

[46] S. W. Park and Y. R. Kim, Interconversion between relaxation modulus and creep compliance for viscoelastic solids, J. Mater. Civ. Eng. **11**, 76 (1999).

[47] H. Leaderman, Viscoelasticity phenomena in amorphous high polymeric systems, in *Rheology*, edited by F. R. Eirich (Academic Press, 1958) pp. 1–61.

[48] E. F. Denby, A note on the interconversion of creep, relaxation and recovery, Rheol. Acta **14**, 591 (1975).

[49] R. Christensen, *Theory of Viscoelasticity*, 2nd ed. (Academic Press, 1982).

[50] H. Winter, Analysis of dynamic mechanical data: inversion into a relaxation time spectrum and consistency check, J. Non-Newtonian Fluid Mech. **68**, 225 (1997).

[51] S. Poudel and S. Shanbhag, Efficient test to evaluate the consistency of elastic and viscous moduli with Kramers–Kronig relations, Korea-Aust. Rheol. J. **34**, 369 (2022).

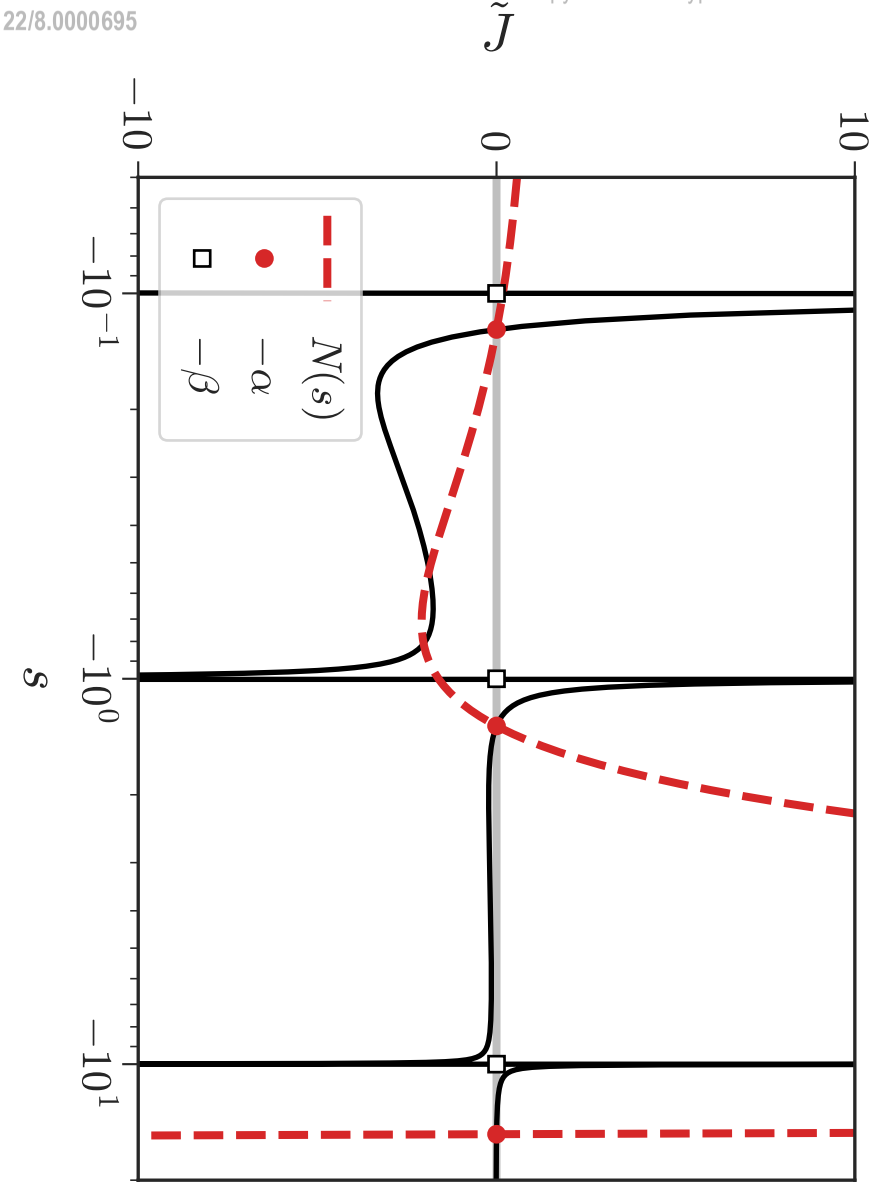

Journal of Rheology

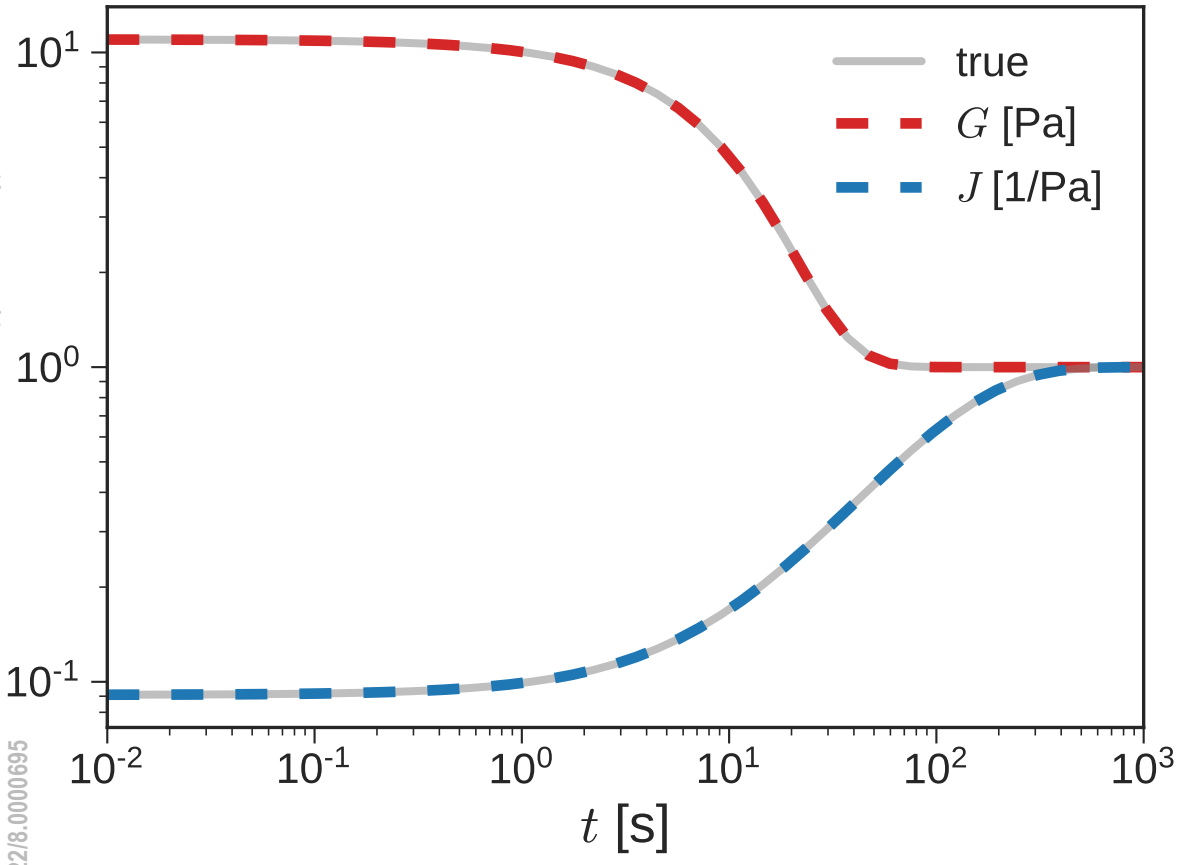

Journal of Rheology

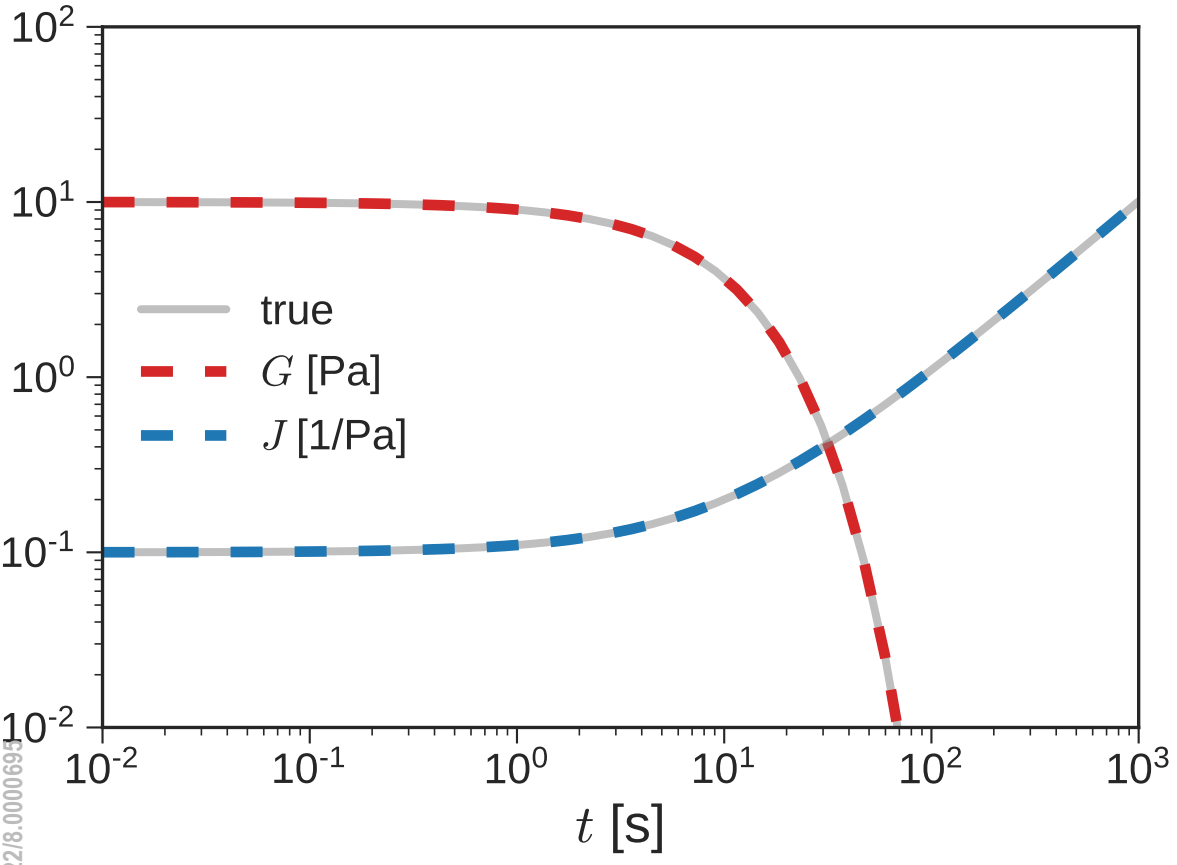

Journal of Rheology

PLEASE CITE THIS ARTICLE AS DOI: 10.1122/8.0000695

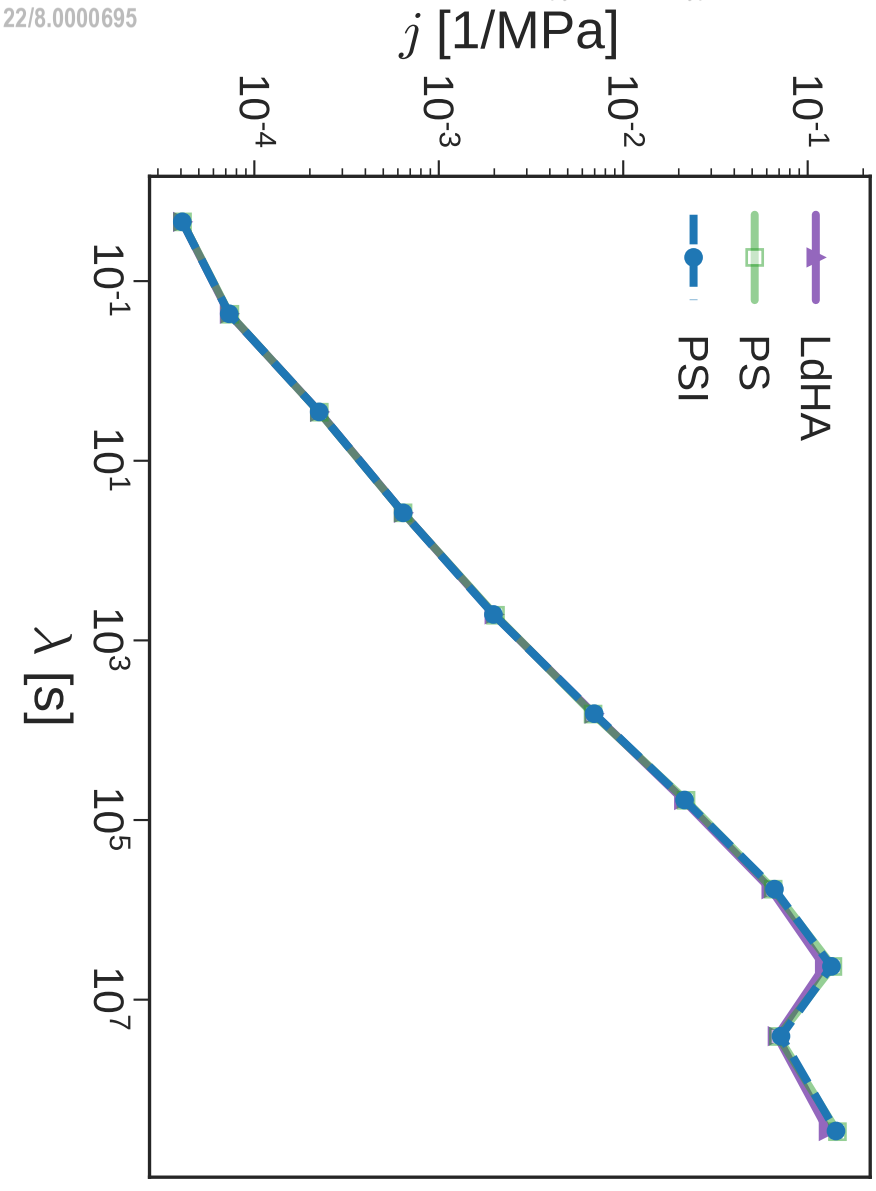

Journal of Rheology

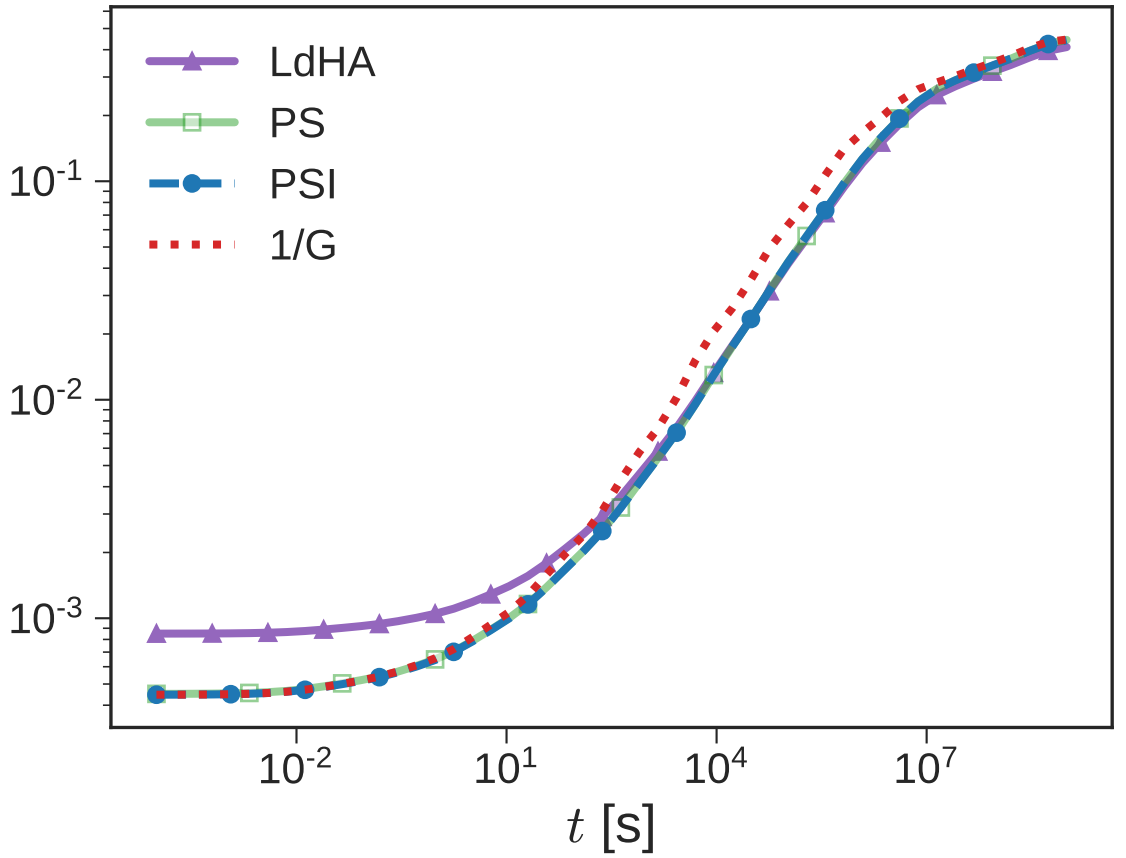

Journal of Rheology

Journal of Rheology

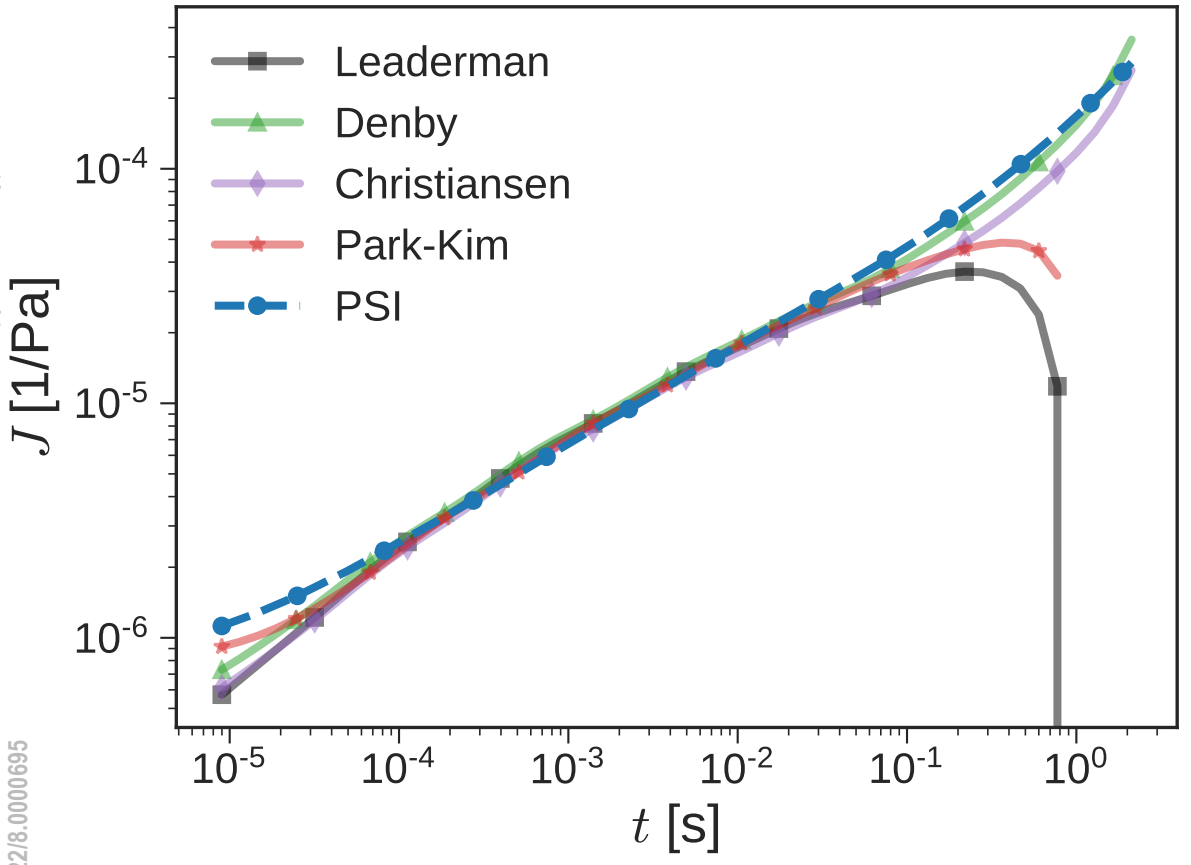

Journal of Rheology

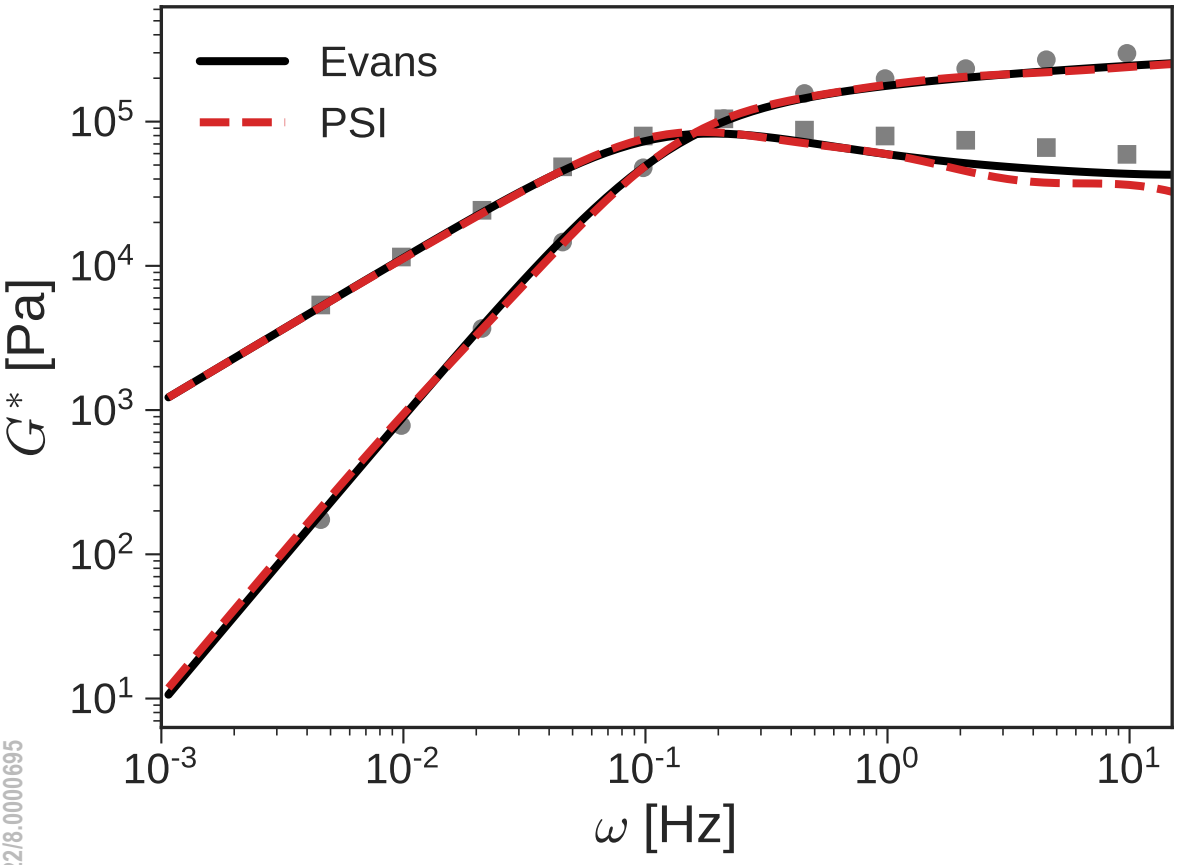

Journal of Rheology